OPO OPHTHALMIC & PHYSIOLOGICAL OPTICS
THE JOURNAL OF THE COLLEGE OF OPTOMETRISTS

Ophthalmic & Physiological Optics ISSN 0275-5408

Bilateral population receptive fields in congenital hemihydranencephaly

Alessio Fracasso[1,2,3], Yvonne Koenraads[4], Giorgio L. Porro[4] and Serge O. Dumoulin[1,3]

[1]Department of Experimental Psychology, Helmholtz Institute, Utrecht University, Utrecht, [2]Department of Radiology, Imaging Division, University Medical Centre, Utrecht, [3]Spinoza Centre for Neuroimaging, Amsterdam, and [4]Department of Ophthalmology, University Medical Centre Utrecht, Utrecht, The Netherlands

Citation information: Fracasso A, Koenraads Y, Porro GL, Dumoulin SO. Bilateral population receptive fields in congenital hemihydranencephaly. *Ophthalmic Physiol Opt* 2016; 36: 324–334. doi: 10.1111/opo.12294

Keywords: functional MRI, hemihydranencephaly, modelling, plasticity, population receptive field, stability

Correspondence: Serge O Dumoulin
E-mail address: S.O.Dumoulin@uu.nl

Received: 14 October 2015; Accepted: 22 February 2016

Abstract

Purpose: Congenital hemihydranencephaly (HH) is a very rare disorder characterised by prenatal near-complete unilateral loss of the cerebral cortex. We investigated a patient affected by congenital right HH whose visual field extended significantly into the both visual hemifields, suggesting a reorganisation of the remaining left visual hemisphere. We examined the early visual cortex reorganisation using functional MRI (7T) and population receptive field (pRF) modelling.
Methods: Data were acquired by means of a 7T MRI while the patient affected by HH viewed conventional population receptive field mapping stimuli. Two possible pRF reorganisation schemes were evaluated: where every cortical location processed information from either (i) a single region of the visual field or (ii) from two bilateral regions of the visual field.
Results: In the patient affected by HH, bilateral pRFs in single cortical locations of the remaining hemisphere were found. In addition, using this specific pRF reorganisation scheme, the biologically known relationship between pRF size and eccentricity was found.
Conclusions: Bilateral pRFs were found in the remaining left hemisphere of the patient affected by HH, indicating reorganisation of intra-cortical wiring of the early visual cortex and confirming brain plasticity and reorganisation after an early cerebral damage in humans.

Introduction

Sensory systems project their afferents towards the central nervous system, keeping their native reference frame in the form of topographic maps. The spatial organisation of these maps follows the organisation of the sensory organ that collects the information, so a spatial code is used for retinotopic maps,[1–3] a tonotopic code for auditory maps[4,5] and so forth. The same type of organisation applies also to efferent parts of the central nervous system, for example the superior colliculus contains, at the level of the tectum, a spatially organised topographic map that controls eye movement direction[6] whereas neighbouring locations control head turns and eye-hand coordination.[7] However, primary afferent and efferent cortices are not the only parts of the central nervous system which are organised topographically: portions of the associative cortex have also been shown to be orderly organised along cognitively relevant dimensions.[8]

The organisation of early visual cortex remains one of the best studied examples of topographic organisation in the central nervous system[1,9–12] where each hemisphere contains several orderly representations of the contra-lateral visual field. Nowadays functional neuroimaging techniques such as functional MRI (fMRI) can routinely localise multiple maps in the early visual cortex *in vivo*.[9–14]

Congenital hemihydranencephaly (HH) represents an extreme case in human development, where only a single brain hemisphere is present.[15–17] The hemispheric loss occurs during prenatal development, mostly due to a vascular insult at the level of one of the carotid arteries[15] which prevents the ipsilateral hemisphere to form and

develop normally. Astonishingly, the destruction of one hemisphere is not always associated with severe neurologic impairments.[17]

As previously reported in a patient affected by HH,[15] standard perimetry assessing the visual field integrity suggested a considerable degree of reorganisation of the visual pathway. The visual field extended across the vertical meridian into visual locations normally processed by the missing hemisphere. This makes this patient affected by HH an extremely interesting model to assess the principles of plasticity and stability that make visual field map representations available for visual perception in humans.[18] Therefore, to study the mechanisms of brain plasticity and stability after an early cerebral damage, population receptive field (pRF) properties of the early visual cortex in a patient affected by HH were measured using fMRI (7T).

In a previous review paper,[18] we drew analogies between the cortical reorganisation of different types of congenital visual pathway disorders, in particular HH, achiasma, and albinism. We suggested that these different conditions may lead to a common type of reorganisation, namely, interleaved representations of both visual hemifields in one hemisphere. At the fMRI resolution, this type of interleaved representations leads to bilateral pRFs in early visual cortex.

FMRI investigation of visual field maps in a previously reported HH case with microphthalmia of the right eye, already showed an overlaid representation of the left and right visual hemifields.[16] However, unlike the previously reported HH case, in the patient affected by HH described in this study both eyes are fully developed, though the left eye is amblyopic, and both project to one hemisphere.

Our case report also differs from albinism, where most of the fibres from each single eye (also fibres from the temporal hemiretina) cross to the contra-lateral lateral geniculate nucleus (LGN) and then project back to the primary visual cortex. Conversely, the patient affected by HH described in this study presents the unique situation in which both visual hemifields and both eyes project to the same hemisphere.

Here, we measure the visual field representation in this unique case of congenital right HH(15), deriving population receptive field properties using functional MRI[1,9–12] and characterising population receptive field (pRF) properties in early visual cortex. Our results show the presence of bilateral population receptive fields in the remaining hemisphere.

Methods

Subjects

All experimental procedures were cleared by the ethics committee of University Medical Centre Utrecht. The patient (age 28) affected by congenital HH was diagnosed after neuroradiological investigation, which was requested because a left hemiplegia was noticed during early neurological examinations. CT and MRI scans of the brain showed that myelination of the left side was normal. The cranium was normal, indicating that the hemisphere originally was formed but was later destroyed, probably by a vascular disruption of the right middle cerebral artery. Torticollis was revealed by early ophthalmological and orthoptic investigations, with the head turned slightly to the left side and tilted towards the left shoulder. The head turn was associated with a left eso- and hypotropia, a latent nystagmus, and a dissociated vertical deviation. Assessment of the ocular motility showed a limitation in the elevation of the left eye. The left eye was mildly amblyopic. To treat it, occlusion on the right eye was prescribed at the age of four, and continued until age eight, then discontinued. Two sessions of strabismus eye surgery were performed, but with little effect on eye and head position. Visual acuity measures (Snellen) were right 6/15 (20/50 or 0.4 decimal) and left 6/38 (~20/130; 0.16 decimal), without correction. Recent visual field measurements are reported in *Figure 1*. Other medical history details: HH patient underwent adenotomy, achilles tendon extension and is treated with Depakine to treat epileptic seizures.

During the current examination, to minimise nystagmus, a patch was applied to the amblyopic eye (left) one hour before the patient affected by HH entered the scanner. During this hour, a visual acuity test of the right eye was performed while the patient was familiarised with the visual stimuli. In addition, her eye movements (right eye) were recorded outside the scanner while viewing the same visual stimuli and maintaining fixation in the centre of the screen. In addition, two healthy control subjects (ages 30 and 32) with normal or corrected-to-normal visual acuity and without any known neurological condition participated in this study.

Visual stimuli setup

Visual stimuli were presented by back-projection onto a 15.0 × 7.9 cm display/screen with resolution of 1024 × 538 pixels inside the MRI bore. HH patients and control subjects viewed the screen/display through prisms and mirrors, and the total distance from the subject's eyes (in the scanner) to the display/screen was 35 cm. Stimuli were generated in Matlab (www.mathworks.com/products/matlab) using the PsychToolbox.[19,20]

Visual stimuli

Stimuli consisted of drifting bar apertures at four orientations, which exposed a checkerboard pattern moving paral-

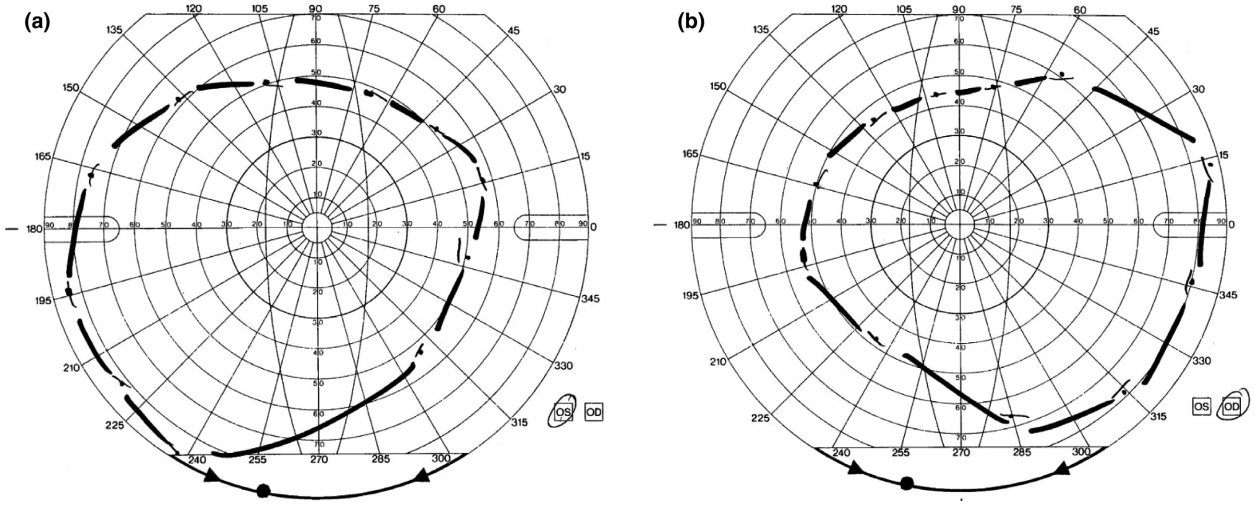

Figure 1. Goldmann kinetic perimetry results from HH (2002). In both the left (panel a) and right (panel b) eyes the visual field extends into left visual hemifield.

lel to the bar orientation.[9–12] Alternating rows of checks moved in opposite directions, and orthogonally with respect to the bar orientation. The bar width (and width of alternating white and black checks) subtended one-quarter of the stimulus radius (1.56 degrees of visual angle). The bar moved across the stimulus aperture in 20 evenly spaced steps, each 0.625 degrees of visual angle, 1/20th of the stimulus window diameter. As there was one step at the start of each functional volume acquisition, each pass of the stimulus lasted 20 acquisition repetitions (TRs), 30 s. Two bar orientations and two different motion directions for each bar were presented, giving a total of four bar motion directions (upward, downward, left and right within each run (the same stimuli order was presented for each run). After each bar pass, a 30 s of mean-luminance (zero contrast) stimulus was displayed. Four mean-luminance blocks were presented at regular intervals during the scan. Subjects fixated on a dot in the centre of the visual stimulus. The fixation dot at the centre of the screen randomly changed colour between green and red, subjects task was to maintain fixation on the point and report the colour change by means of a button press.

Structural and functional data acquisition

One structural T1-weighted anatomical MRI scan was acquired with a resolution of 0.8 × 0.8 × 0.8 mm. Repetition time (TR) was 7 ms, echo time (TE) was 2.84 ms and flip angle was 8 degrees acquired after the functional data acquisition (*Figure 2a*).

Functional T2*-weighted multi-slice echo-planar images (EPI) were acquired in two separate sessions (two different days, for HH patient) and in a single acquisition (control subjects) using a Philips Achieva 7T scanner (Best, Netherlands), a volume transmit coil for excitation and a 32-channel head coil for signal reception (Nova Medical, MA, USA). Acquisition parameters were: TR/TE: 1500/30 ms, flip angle: 70°, voxel size: 2 mm isotropic, and 24 coronal slices, centred on the occipital pole. Functional scans were each 168 time frames (252 s) in duration.

Preprocessing

For each session, EPI images were motion corrected for head movement between scan acquisitions using the 3dvolreg function in AFNI (http://afni.nimh.nih.gov), using 6 degrees of freedom. For the HH patient the two motion-corrected EPI sessions were co-registered in the same space using the 3dAllineate function in AFNI. Motion corrected images were co-registered with the T1-weighted anatomical scan using the mrVista software (https://github.com/vistalab/vistasoft). T1-weighted anatomical scans were resampled to 1 mm^3 resolution. The resulting anatomical image was manually segmented delineating white matter and grey matter.

Functional data analysis

Population receptive field sizes and positions were estimated from the fMRI data and visual stimulus position time course and the BOLD (blood oxygen level dependent) response of each voxel was predicted using a 2D Gaussian pRF model with three different parameters[18,21]: pRF position (x and y parameters) and spread (σ). The predicted fMRI time course was calculated by convolution of the

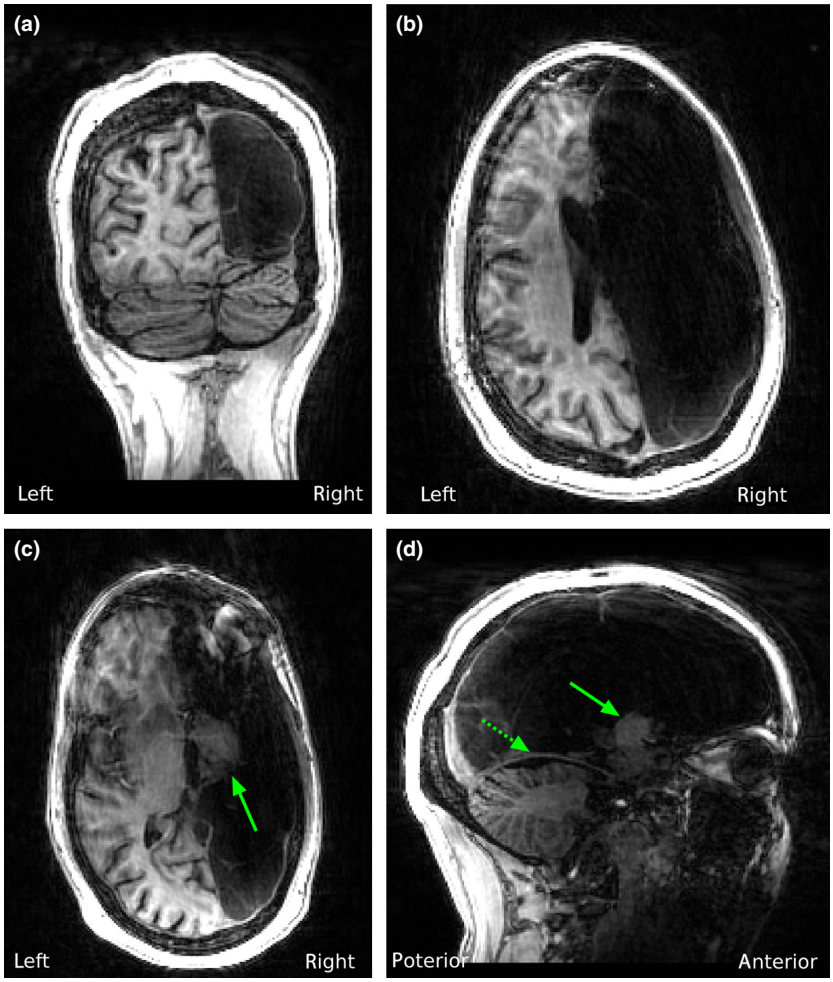

Figure 2. Structural MRI of the patient affected by HH. Panels (a,b) coronal and horizontal slice illustrating the HH of the right hemisphere. Panel (c) horizontal and sagittal slices showing the partially spared ipsilateral thalamus (continuous arrow). Panel D: partially spared ipsilateral thalamus (continuous arrow) and, as a reference, the tentorium indicated by the dotted arrow.

modelled pRF, the stimulus sequence, and a canonical BOLD hemodynamic response function (HRF).[22] The pRF parameters for each voxel are determined by minimising the sum of squared errors (RSS) between the predicted and observed fMRI time series. The proportion of variance explained for each voxel was stored and saved for further analysis (see *Model Comparison*).

For each subject (patient affected by HH and control subjects), three different models were tested: a single 2D Gaussian pRF (single pRF), a model in which 2D Gaussians were mirrored around the horizontal axis (bilateral pRF, mirrored around the horizontal meridian) and a model in which 2D Gaussians model were mirrored around the vertical axis (bilateral pRF, mirrored around the vertical meridian). Because the two Gaussians are linked to each other, these models have the same degrees of freedom as the conventional one Gaussian pRF model. Unlike the conventional model, these models represent two separate regions of visual space within each cortical location.[9,21]

Eye movement recording

Eye movements during stimulus presentation can affect the pRF sizes estimated.[23] Eye movements of the HH patient were measured using an Eyelink II system (SR Research, http://www.sr-research.com/) before entering the scanner. This allowed us to measure the distribution of fixation positions with the same stimulus and task as was shown in the scanner.

Control subjects and additional experimental conditions

The two healthy control subjects were presented with two experimental conditions. In the first experimental condi-

tion (fixation condition), the central fixation point remained fixed in the centre of the screen during the whole duration of the run and subjects were asked to report a change in fixation point colour (from red to green and vice-versa). In the second experimental condition (eye movement condition) the central fixation point moved following the trajectory recorded offline (outside the scanner) of the HH patient. Also in this second experimental condition, subjects were asked to report a change in fixation point colour (from red to green and vice-versa). By asking the subjects to perform similar eye movements, we aimed to match the visual input experienced by the HH patient in our healthy control subjects. However, because we did not expect the healthy control subjects to follow exactly the fast and erratic eye movement trajectories on the screen, we ran two additional controls for eye movements. We estimated pRF properties in healthy control subjects' data (in the fixation condition) using a jittered version of the visual input: (i) according to the eye movement data measured on the HH patient and (ii) artificially doubling the amplitude of the measured eye movements.

Model comparison

For each model, pRFs fits below 12% variance explained were excluded from further analysis. The conjunction of the voxels that survived the thresholding for each separate model entered the subsequent stage of analysis. In this way the same recording sites for each model were evaluated.

The three models were compared in pairs (three different comparisons) for each dataset by means of signal detection theory.[24] For each model comparison the variance explained distribution of the first model was taken as the test distribution, whereas the variance explained of the second model was taken as baseline distribution. Iso-sensitivity lines (lines of identical sensitivity) between the two distributions were derived by changing iteratively the threshold variance explained and computing the false-alarm rate (FA) and hit-rate (HIT) associated with the baseline and test distributions. For each model comparison the area under the curve (AUC) was computed to summarise which model better predicted the observed data. AUC values above 0.5 indicated that the test model predicted the data better than the baseline model. A value of 0.5 indicated that the test model and baseline models could not be separated (explained the data equally well). AUC values below 0.5 indicated that the test model predicted the data worse than the baseline model. AUC Bonferroni corrected 95% confidence intervals (CI) were computed for each model comparison by bootstrapping the baseline and test distribution 2000 times with replacement. The empirical confidence interval of the parameter of interest was corrected according to the number of condition tested.

PRF size vs eccentricity relationship

PRF eccentricity was binned into 10 equally spaced intervals from 0.25 until 5.25 degrees of visual angle (adeg), the median pRF size was computed for each eccentricity bin and the relationship between the binned pRF size and eccentricity was tested by means of a linear model as done in previous reports.[1–3,9–12] Bonferroni corrected 95% confidence intervals (CI) were computed for each model by bootstrapping PRF size and eccentricity estimates 2000 times with replacement. The empirical confidence interval of the parameter of interest was corrected according to the number of condition tested. For example in *Figure* 5*a* there are empirical 95% confidence intervals reported for seven different conditions, thus each confidence interval comes from the .05/7 and 1-.05/7 quantiles of the parameter of interest (in this case, AUC).

Results

HH behavioural performance

Performance of the patient affected by HH on the behavioural task presented at fixation exceeded 70% and 80% correct both inside and outside the MR scanner, respectively. This performance indicates that our HH patient was fixating and able to successfully report the majority of fixation colour changes. Eye movement recording outside the MR scanners confirmed the presence of latent nystagmus in the range of 3–4 degrees of visual angle, with a frequency of ~0.75 Hz.

Severe movements inside the MR environment limited analyses

Subject movement inside the scanner not only introduces displacement of the signal source but also magnetic field distortions,[25] which will corrupt the signal integrity. Furthermore, motion correction techniques can only account for movement between different fMRI images (acquired at each separate TR), whereas motion within a TR cannot be corrected for (e.g. tremor within a single TR). The HH patient moved substantially within the MR scanner. Motion detection and correction algorithms estimated this motion to be on the order of 8–9 degrees for rotations and 7 mm for translations across a whole session. In comparison, displacement in the order of 1–2 degrees or 2–3 mm are already considered problematic to correct for at the within-subject level, with the risk of ending in local-minima of the cost function, resulting in very poor motion correction.[26] This amount of motion forced us to discard the majority of the functional data collected and limit the analysis to the first functional run of each acquisition session (*Figure 3*), similar results were obtained

using different motion correction cost functions.[26] The motion estimated in the selected two runs was in the order of 1.5 degrees for rotations and 1.3 mm for translation, comparable with that observed in control subjects. The two runs were averaged together to increase signal-to-noise ratio (SNR). Given that only two runs were available for the HH patient, we limited the analysis to two runs only also for the healthy control subjects analysis, in each experimental condition (fixation and eye movements). Overall, variance explained for the HH patient dataset was lower than those observed with the healthy control subjects.

The severe subject motion confounded any conventional analyses of visual field map organisation on the cortex surface, as usually done in retinotopic mapping and pRF mapping studies 9–14. Instead, we compared the results across different models (see *Methods* → *Model Comparison* section[21]).

By limiting the analysis to those scans with an acceptable amount of motion and thoroughly testing for eye movement artefacts (see *Control Subjects, Experimental Conditions*) we limited the influence of unwanted covariates, potentially affecting our results.

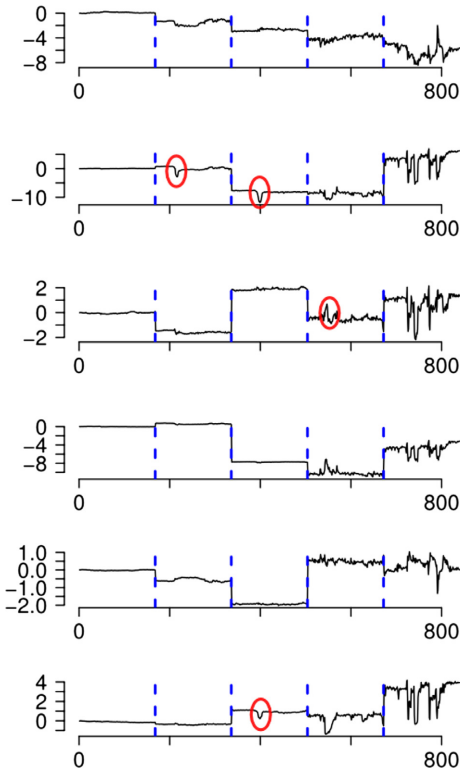

Figure 3. Motion correction results from the patient with HH from the first session. Separate subplots report six motion parameters, from top to bottom: rotation about the inferior-superior axis (degrees), rotation about the left-right axis (degrees), rotation about the anterior-posterior axis (degrees), translation in the superior direction (mm), translation in the left direction (mm), translation in the posterior direction (mm). *X* axis reports time in seconds, blue dotted lines indicates different runs. Red circles indicate events with sudden, erratic motion. We were forced to discard the majority of the functional data collected and limit the analysis to the first functional run of each acquisition session (data from a second session on a different day showed a similar pattern).

Bilateral pRFs in the patient affected by HH but not control subjects

We compared all MRI recording sites that survived a minimum variance explained (R^2) value of 12% for any model. We evaluated the models using iso-sensitivity curves (*Figure 4*). The iso-sensitivity curves highlight an atypical pattern of results in the HH patient (*Figure 4*, orange line). The bilateral pRF mirrored around the vertical axis outperformed the single pRF model, whereas the opposite pattern of results could be observed in control subjects, with single pRF model performing better than bilateral pRF model (*Figure 4*, blue and green lines).

We visualised different conditions in one figure (*Figure 4*): if the iso-sensitivity line was above the bisection line (dotted line, *Figure 4*), then the bilateral pRF model (mirrored around the vertical axis) performed better than the single pRF model. This results in AUC larger than 0.5. Similarly, if the iso-sensitivity line was below the bisection line (*dotted line, Figure 4*), then the single pRF model performed better than the bilateral pRF model (mirrored around the vertical axis). In this case, the AUC is smaller

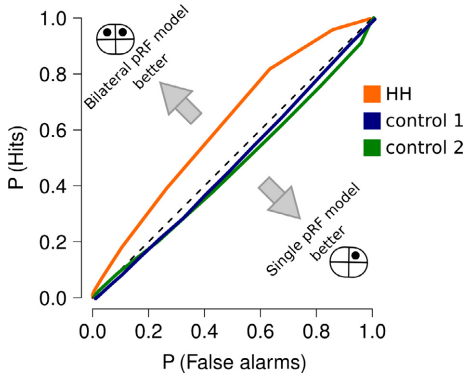

Figure 4. Comparison between bilateral pRF model (mirrored around the vertical axis) and single pRF model. Iso-sensitivity lines for the model comparisons are reported. On the data acquired from the subject affected by HH, bilateral pRF model (mirrored around the vertical axis) outperformed the single pRF model (black line). Control subjects show the opposite pattern, single pRF model performs better than bilateral pRF model (mirrored around the vertical axis, grey lines). Dotted line represents bisection, where bilateral pRF model and single pRF model cannot be distinguished. The icons represent schematic pRFs visual field configurations.

than 0.5. In case the line follows the bisection line (*dotted line, Figure 4*) then the single pRF model and the bilateral pRF model (mirrored around the vertical axis) could not be separated (both models explained the data equally well), i.e. AUC equals 0.5. Our result demonstrates that the bilateral pRF model outperforms the conventional single pRF model on the subject affected by HH but not controls.

For each model comparison we computed the AUC for the iso-sensitivity line, to summarize which model better predicted the observed data (*Figure 5*). The bilateral pRF, mirrored around the vertical axis, outperformed the single pRF model for the HH patient, but the opposite pattern was observed on healthy control subjects results at fixation, when asked to perform an eye movement and when the model input was jittered according to eye movements recorded offline on the HH patient (*Figure 5a*). Similar results could be observed on the comparison between the bilateral pRF, mirrored around the vertical axis and the single pRF model and bilateral pRF, mirrored around the horizontal axis (*Figure 5b*). As a further control, AUC on bilateral pRF, mirrored around the horizontal performed worse than single pRF model, across all tested datasets (*Figure 5c*). The same pattern of results could be observed also when we artificially double the amount of the visual input jittering on control subjects (twice as much than what was recorded offline on the patient affected by HH, data not shown).

Several techniques are available to analyse pRF mapping data.[27] Some of them show benefits compared to the classic model-based approach,[27,28] for example being less influenced by the high degree of correlated response patterns that pRF mapping elicits. The approach adopted in our experiment directly build upon from already published research, where bilateral pRFs were found on an achiasmatic patient, using the same technique adopted here.[18,21] PRF positions were mirrored with respect to the vertical (or horizontal meridian) to keep a constant number of model parameters between the single Gaussian and the bilateral pRFs models. Otherwise the number of degrees of freedom would differ between the different models, which will complicate the comparison between different models.

It can be argued that if the data quality is poorer, it is more likely that the bilateral pRF model will fit the data better despite both models having the same degrees of freedom. For this reason, we tested two bilateral pRFs configurations (bilateral, mirrored around the vertical axis vs bilateral, mirrored around the horizontal axis, (*Figure 5b*). We observed an advantage of the bilateral vertical pRF model compared to the bilateral horizontal pRF for the HH patient. Even when comparing models with very similar

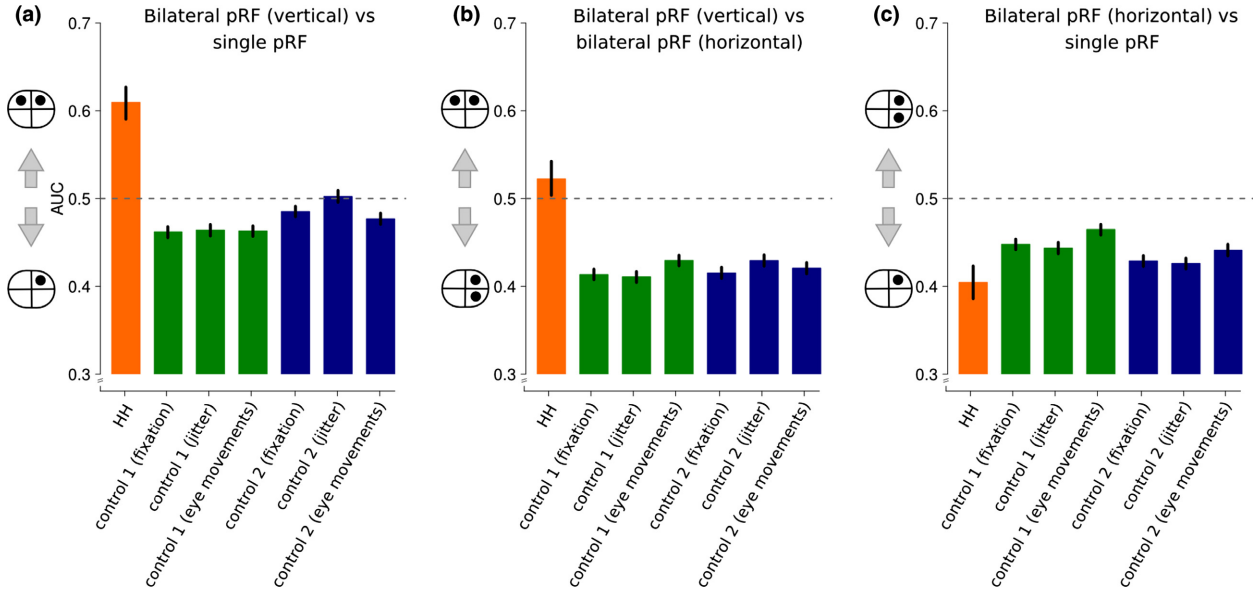

Figure 5. AUC comparison between different models. The error bars indicate the AUC 95% CI (Bonferroni corrected). Panel (a) The bilateral pRFs mirrored around the vertical axis outperformed the single pRF model for the HH patient (orange bar). This was not the case for control subjects, neither when fixating nor while making eye-movements nor when the model input was jittered according to eye movements recorded on the HH patient (blue and green bars). Panel (b) The bilateral pRF, mirrored around the vertical axis outperformed the bilateral pRF, mirrored around the horizontal axis, for the HH patient (orange bar). Again, this was not the case for control subjects' results, along all experimental conditions tested (blue and green bars). Panel (c) A different biologically-implausible bilateral pRF model where the pRFs were mirrored around the horizontal axis performed worse than the single pRF model in all tested datasets. Icons represents schematic pRFs visual field configurations. These results demonstrate that the bilateral pRF model outperforms any other model in the HH patient but not in control subjects and several control conditions.

features within the same dataset (hence, with the same level of noise), the bilateral pRF model mirrored around the vertical meridian outperforms the alternatives.

pRF size vs eccentricity relationships

Only when taking into account bilateral pRFs, mirrored along the vertical axis, the HH patient showed a significant and expected increase of pRF size with increase eccentricity (*Figure 6a, slope estimate = 0.34, t = 8.80, p < 0.001*). This result was confirmed by the bootstrapped 95% confidence intervals of the slope parameter: [0.09 0.45]. This is analogous to our observation in achiasmic patients.[21] We did not observe this pattern for other pRF models: bilateral pRF, mirrored along the horizontal axis: slope estimate = −0.09, $t = -1.45$, *ns;* single pRF: slope estimate = −0.01, $t = -0.33$, ns). On the other hand, the bootstrapped 95% confidence intervals of the slope parameter did not differ significantly between the different pRF models (bilateral pRF, mirrored along the horizontal axis: [−0.81 0.18]; single pRF: [−0.5 0.15]). So we see a trend of typical pRF size vs eccentricity in the bilateral pRFs even though not as strong as the ones observed in healthy populations. We could observe the same pRF size vs eccentricity relationship in control subjects for the pRF model with single location, as it is known to occur[9–12,29–34] (fixation condition, *Figure 6d*, slope estimate = 0.24, $t = 49.25$, $p < 0.001$). Healthy control subjects showed overall larger pRF sizes than the HH patient (*Figure 6,* panel *a, b,* $t = 29.56$, $p < 0.001$). This may be a difference between controls and HH. On the other hand, even in healthy control subjects, pRF sizes vary with a factor of two.[10] Consequently, this difference may also be attributed to normal variation between subjects.

Our results shows an atypical organisation of early visual cortex in a patient affected by congenital right HH. The data reveals an overlaid representation of both right and left visual hemifield located in the occipital lobe of the contralesional hemisphere of the HH patient. The AUC analysis suggests that pRFs consists of bilateral pRFs, mirrored around the vertical axis. Furthermore, the biologically known relationship between pRF size and eccentricity was only recovered when taking into account this atypical model with bilateral pRFs. This strongly suggests bilateral

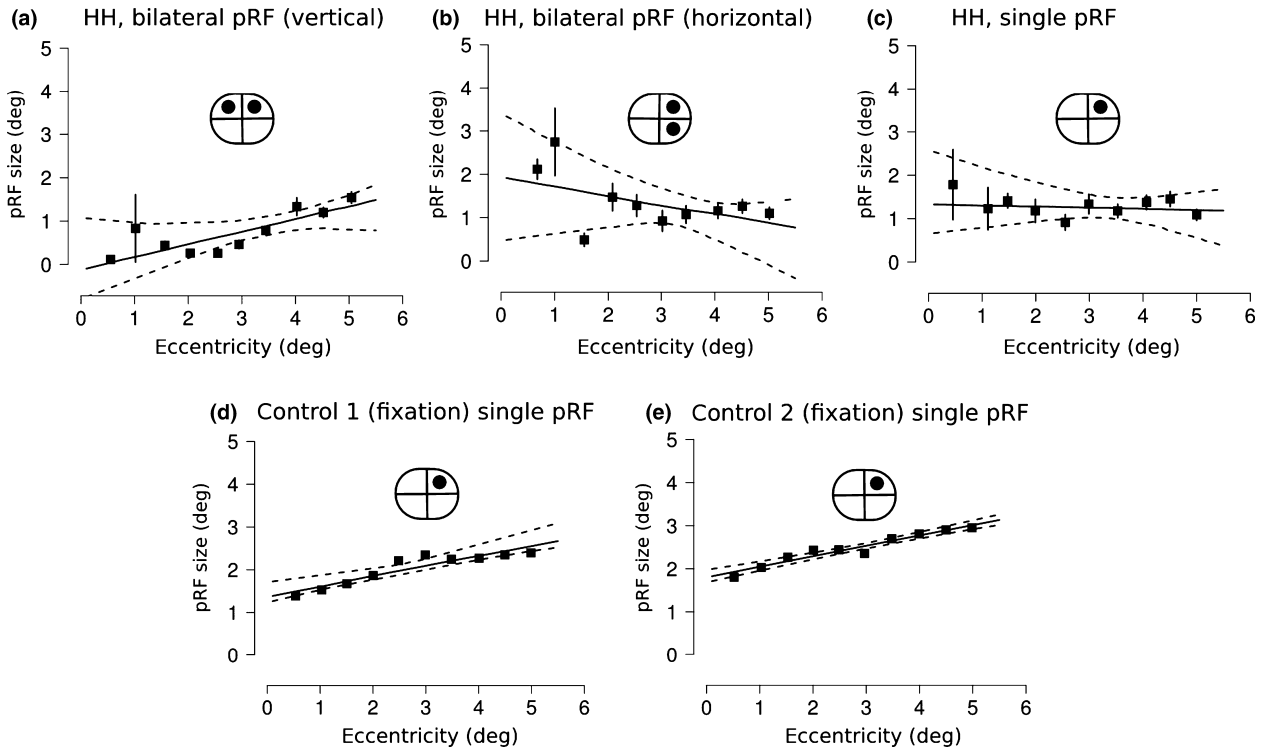

Figure 6. PRF size vs eccentricity relationship. Panel (a) Data on the HH patient showed the expected pRF size vs eccentricity relationship only when data was fit with the model with bilateral pRFs, mirrored around the vertical axis. Panel (b) The HH patient did not show the expected pRF size vs eccentricity relationship when data was fit with bilateral pRFs, mirrored around the horizontal axis. Panel (c) The HH patient did not show the expected pRF size vs eccentricity relationship when data was fit with single pRFs. Panels (d,e) PRF size vs eccentricity relationship in healthy control subjects. The same pattern could be observed in existing studies[9–12] with the single pRF. Icons represents schematic pRFs visual field configurations. This data illustrates normal pRF size relationships in HH patient only when taking into account the abnormal bilateral pRF model.

pRFs and overlapping visual field maps in this HH patient. This provides further evidence for the hypothesis that, in humans, these types of congenital visual pathway malformations result in an interleaved representation of the ipsi- and contralateral visual field in early visual cortex.[16,21] These results differ from studies on other non-human primates, in the case of congenital chiasmatic abnormalities, where three different reorganisation schemes have been observed.[18,35,36]

Hard wired topographical representation and hemihydranencephaly

Congenital hemihydranencephaly provides an interesting case to evaluate the plasticity and stability mechanisms operating during neonatal development. Rat studies suggest that the development of topographical organisation of early visual cortex is an hard-wired process: during normal development, neighbouring neurons in the retina project to neighbouring neurons in the LGN that grow their axons until they reach V1 neurons.[37,38] A dramatic vascular event, such the one that prevents the formation of a whole hemisphere,[15,17] forces a rewiring of the formation of early topographical organisation. PRF mapping results shows an overlaid, or interleaved, representation of both the right and left visual hemifields in the occipital lobe of the contralesional hemisphere in the HH patient.

For each cortical location two separate visual field locations are represented simultaneously, one on each single hemifield. Two non-mutually exclusive configurations might drive this type of result: individual neurons could be characterised by bilateral receptive fields. Namely, a single neuron can be sensitive to two separated location in space, mirrored with respect to the vertical meridian.[21] Alternatively, intermixed neuronal populations each sensitive to one location in visual space may underlie bilateral pRFs.

During embryo development the crossing of the optic nerve fibres towards the contralateral side is mediated by molecular cues[39] and occurs approximately after 50 days of gestation.[40] It is likely that the vascular insult that prevented the formation of the missing hemisphere had already occurred when the optic nerve fibres reached the chiasm crossing during embryo development. In those conditions the fibres from the contralateral eye followed only contra-lateral molecular cues due to the lack of ipsi-lateral guiding cues. This is consistent with the anatomical images, showing a spared contra-lateral thalamus and a partially spared ipsi-lateral thalamus.

A redirection of the eye-LGN projection to the surviving hemisphere as the one described above, together with a preserved geniculostriate projection, would yield an intermixed neuronal population where each neuron is sensitive to one location in visual space. This pattern of rewiring at the level of the thalamus likely underlie the reorganisation that we observe from the functional data in HH primary visual cortex, and it is consistent with what has been reported in cases of human hemihydranencephalia and achiasma.[16,21]

Thus this result is consistent with a reorganisation of the input to the thalamus, whereas thalamo-cortical projections are preserved but carrying different information. Therefore, akin to achiasma, we suggests that local intracortical reorganisations make the altered visual field representation available for perception.

Hemihydranencephaly in comparison with other visual pathway disorders

The data reported confirms finding of Muckli *et al.* on HH.[16] We extend and complemented their observations in two important ways. First, Muckli *et al.* in their previous report on HH did not evaluate the presence of bilateral pRFs directly. Though their overlapping visual field maps is suggestive of this in part. In our HH patient we extended the previous findings testing separate models via a forward-modelling approach and testing alternative re-organisation models to the same dataset. Second, the HH patient described by Muckli *et al.*[16] was not only hemihydranencephalic but also anophthalmic in the right eye, a situation more comparable to achiasma where one eye projects to one hemisphere. On the contrary, in our HH patient, both eyes project visual information into the same hemisphere; despite one eye being amblyopic. Obviously, amblyopia *per se* does not result in bilateral pRFs.[41] Also, the reported HH case differs from previous cases of achiasma[21] and albinism,[42] given that in the present investigation, a single hemisphere processes not only both visual hemifields but also both eyes.

In the HH patient tested here, both eyes and hemifields converge towards a single hemisphere, hence the rewiring involved may differ from the previous case report of HH.[16] Yet, the results are consistent with the type of rewiring observed in completely different cases of abnormal visual pathways, such as achiasma[21] and albinism.[42] However, differences might arise at a smaller scale (finer spatial resolution) than the one measured so far with functional neuroimaging in the current investigation and others.[16] The investigation on rewiring mechanisms occurring during neonatal stage would benefit from current improvements in high-field functional imaging at sub-millimetre resolution.[18]

Behaviour

A recent review on hemihydranencephaly form Pavone *et al.*[17] shows that, quite surprisingly, this brain's anomaly

is not frequently associated with language problems or severe mental retardation, and confirm that often cognitive performance and visual function are relatively preserved (except for nystagmus and lack of stereopsis). Also consistent with the reviewed cases of Pavone *et al.*,[17] also the HH patient tested here made effective use of her vision in daily life, with no apparent confusion between left and right visual fields. This observation is in line with what has been observed in subjects with achiasma.[43–45]

Conclusions

The study of visual pathway abnormalities is a powerful model for our basic understanding of developmental mechanisms in the human brain, and provides crucial insight into the relation between stability and plasticity in the human visual system. The fMRI results described in this study on a patient affected by congenital HH, complemented with previous ophthalmological investigations demonstrate the high degree of plasticity of the visual system at the stage of neonatal development. Despite the severe anatomical abnormalities, the visual system of HH seems to create successfully adaptations in order to obtain a stable visual representation[15,18] and shows an interleaved representation of the ipsi- and contralateral visual fields in early visual cortex.

In conclusion, this study lends further evidence to the hypothesis that in humans congenital visual pathway malformations, such as hemihydranencephaly, achiasma, and albinism, developmental mechanisms of local wiring within cortical maps compensate for the improper gross wiring to preserve visual function.[18]

Disclosure

There are no conflicts of interest.

Acknowledgments

This work was supported by a Netherlands Organisation for Scientific Research (NWO) Grant 433.09.223 (S.O.D.). The Spinoza Centre is a joint initiative of the University of Amsterdam, VU University, Academic Medical Centre, VU Medical Centre, Netherlands Institute for Neuroscience and the Royal Netherlands Academy of Arts and Sciences.

References

1. Wandell BA, Dumoulin SO & Brewer AA. Visual field maps in human cortex. *Neuron* 2007; 56: 366–383.
2. Inouye T. *Die Die Sehstörungen bei Schussverletzungen der Kortikalen Sehsphäre Nach Beobachtungen an Verwundeten der Letzten Japanischen Kriege*, Engelmann: Leipzig, 1909.
3. Holmes G. Disturbances of visual orientation. *Br J Ophthalmol* 1918; 2: 506–516.
4. Merzenich MM & Brugge JF. Representation of the cochlear partition of the superior temporal plane of the macaque monkey. *Brain Res* 1973; 50: 275–296.
5. Talavage TM, Sereno MI, Melcher JR, Ledden PJ, Rosen BR & Dale AM. Tonotopic organization in human auditory cortex revealed by progressions of frequency sensitivity. *J Neurophysiol* 2004; 91: 1282–1296.
6. Klier EM, Wang H & Crawford JD. The superior colliculus encodes gaze commands in retinal coordinates. *Nat Neurosci* 2001; 4: 627–632.
7. Klier EM, Wang H, Constantin AG & Crawford JD. Midbrain control of three-dimensional head orientation. *Science* 2002; 295: 1314–1316.
8. Harvey BM, Klein BP, Petridou N & Dumoulin SO. Topographic representation of numerosity in the human parietal cortex. *Science* 2013; 341: 1123–1126.
9. Dumoulin SO & Wandell BA. Population receptive field estimates in human visual cortex. *NeuroImage* 2008; 39: 647–660.
10. Harvey BM & Dumoulin SO. The relationship between cortical magnification factor and population receptive field size in human visual cortex: constancies in cortical architecture. *J Neurosci* 2011; 31: 13604–13612.
11. Zuiderbaan W, Harvey BM & Dumoulin SO. Modeling center-surround configurations in population receptive fields using fMRI. *J Vis* 2012; 12(3): 1–10.
12. Amano K, Wandell BA & Dumoulin SO. Visual field maps, population receptive field sizes, and visual field coverage in the human MT+ complex. *J Neurophysiol* 2009; 102: 2704–2718.
13. Sereno MI, Dale AM, Reppas JB *et al.* Borders of multiple visual areas in humans revealed by functional magnetic resonance imaging. *Science* 1995; 268: 889–893.
14. Engel SA, Rumelhart DE, Wandell BA *et al.* fMRI of human visual cortex. *Nature* 1994; 369: 525.
15. Porro G, Wittebol-Post D, de Graaf M, van Nieuwenhuizen O, Schenk-Rootlieb AJ & Treffers WF. Development of visual function in hemihydranencephaly. *Dev Med Child Neurol* 1998; 40: 563–567.
16. Muckli L, Naumer MJ & Singer W. Bilateral visual field maps in a patient with only one hemisphere. *Proc Natl Acad Sci USA* 2009; 106: 13034–13039.
17. Pavone P, Nigro F, Falsaperla R *et al.* Hemihydranencephaly: living with half brain dysfunction. *Ital J Pediatr* 2013; 39: 3.
18. Hoffmann MB & Dumoulin SO. Congenital visual pathway abnormalities: a window onto cortical stability and plasticity. *Trends Neurosci* 2015; 38: 55–65.
19. Brainard DH. The psychophysics toolbox. *Spat Vis* 1997; 10: 433–436.
20. Pelli DG. The VideoToolbox software for visual psychophysics: transforming numbers into movies. *Spat Vis* 1997; 10: 437–442.

21. Hoffmann MB, Kaule FR, Levin N *et al.* Plasticity and stability of the visual system in human achiasma. *Neuron* 2012; 75: 393–401.
22. Friston KJ, Fletcher P, Josephs O, Holmes A, Rugg MD & Turner R. Event-related fMRI: characterizing differential responses. *NeuroImage* 1998; 7: 30–40.
23. Levin N, Dumoulin SO, Winawer J, Dougherty RF & Wandell BA. Cortical maps and white matter tracts following long period of visual deprivation and retinal image restoration. *Neuron* 2010; 65: 21–31.
24. Macmillan NA & Creelman CD. *Detection Theory: A User's Guide*, 2nd edn, Lawrence Erlbaum Assoc: New Jersey, 2004.
25. Friston KJ, Williams S, Howard R, Frackowiak RS & Turner R. Movement-related effects in fMRI time-series. *Magn Reson Med* 1996; 35: 346–355.
26. Saad ZS, Glen DR, Chen G, Beauchamp MS, Desai R & Cox RW. A new method for improving functional-to-structural MRI alignment using local Pearson correlation. *NeuroImage* 2009; 44: 839–848.
27. Lee S, Papanikolaou A, Logothetis NK, Smirnakis SM & Keliris GA. A new method for estimating population receptive field topography in visual cortex. *NeuroImage* 2013; 81: 144–157.
28. Greene CA, Dumoulin SO, Harvey BM & Ress D. Measurement of population receptive fields in human early visual cortex using back-projection tomography. *J Vis* 2014;14: pii: 17.
29. Burkhalter A & Van Essen DC. Processing of color, form and disparity information in visual areas VP and V2 of ventral extrastriate cortex in the macaque monkey. *J Neurosci Off J Soc Neurosci.* 1986; 6: 2327–2351.
30. Felleman DJ & Van Essen DC. Receptive field properties of neurons in area V3 of macaque monkey extrastriate cortex. *J Neurophysiol* 1987; 57: 889–920.
31. Gattass R, Sousa APB & Rosa MGP. Visual topography of V1 in the Cebus monkey. *J Comp Neurol* 1987; 259: 529–548.
32. Newsome WT, Maunsell JH & Van Essen DC. Ventral posterior visual area of the macaque: visual topography and areal boundaries. *J Comp Neurol* 1986; 252: 139–153.
33. Rosa MGP, Sousa APB & Gattass R. Representation of the visual field in the second visual area in the Cebus monkey. *J Comp Neurol* 1988; 275: 326–345.
34. Van Essen DC, Newsome WT & Maunsell JH. The visual field representation in striate cortex of the macaque monkey: asymmetries, anisotropies, and individual variability. *Vision Res* 1984; 24: 429–448.
35. Hoffmann MB, Tolhurst DJ, Moore AT & Morland AB. Organization of the visual cortex in human albinism. *J Neurosci Off J Soc Neurosci* 2003; 23: 8921–8930.
36. Guillery RW. Neural abnormalities of albinos. *Trends Neurosci* 1986; 9: 364–367.
37. Espinosa JS & Stryker MP. Development and plasticity of the primary visual cortex. *Neuron* 2012; 75: 230–249.
38. Kanold PO & Luhmann HJ. The subplate and early cortical circuits. *Annu Rev Neurosci* 2010; 33: 23–48.
39. Lambot M-A, Depasse F, Noel J-C & Vanderhaeghen P. Mapping labels in the human developing visual system and the evolution of binocular vision. *J Neurosci Off J Soc Neurosci* 2005; 25: 7232–7237.
40. Kerwin J, Scott M, Sharpe J *et al.* 3 dimensional of early human brain development using optical projection tomography. *BMC Neurosci* 2004; 5: 27.
41. Barnes GR, Hess RF, Dumoulin SO, Achtman RL & Pike GB. The cortical deficit in humans with strabismic amblyopia. *J Physiol* 2001; 533: 281–297.
42. Kaule FR, Wolynski B, Gottlob I *et al.* Impact of chiasma opticum malformations on the organization of the human ventral visual cortex. *Hum Brain Mapp* 2014; 35: 5093–5105.
43. Apkarian P, Bour L & Barth PG. A unique achiasmatic anomaly detected in non-albinos with misrouted retinal-fugal projections. *Eur J Neurosci* 1994; 6: 501–507.
44. Apkarian P, Bour LJ, Barth PG, Wenniger-Prick L & Verbeeten B. Non-decussating retinal-fugal fibre syndrome. An inborn achiasmatic malformation associated with visuotopic misrouting, visual evoked potential ipsilateral asymmetry and nystagmus. *Brain* 1995; 118: 1195–1216.
45. Prakash S, Dumoulin SO, Fischbein N, Wandell BA & Liao YJ. Congenital achiasma and see-saw nystagmus in VACTERL syndrome. *J Neuro-Ophthalmol* 2010; 30: 45–48.